THE USE OF LANDSAT IMAGERY TO DOCUMENT LAND USE CHANGES IN THE GALVESTON BAY AREA, TEXAS

Sarah E. Robinson
Department of Geosciences
Franklin and Marshall College
Lancaster, Pennsylvania

Matthew Nwosu
Department of Geosciences
Colgate University
Hamilton, New York

INTRODUCTION

The focus of this project was to use Landsat thematic imagery to analyze land use changes. This project focused on the Galveston Bay area on the coast of Texas; this area was chosen because both man made features and natural environments are present. Processing techniques, such as clustering and supervised classification, were used to create a thematic map. The goal of this project was to determine the urban growth over approximately a decade by comparing the thematic maps from the 1985 image to earlier maps of the area.

IMAGE PROCESSING

This project processed a Landsat image of the Galveston Bay area. From the raw Thematic Mapper (TM) bands, a 3,2,1 true-color and a 4,3,2 false-color, infra-red composite were created. The 4,3,2 composite was used to highlight the difference between vegetated and urban areas. This combination was also particularly useful in defining water boundaries and differentiating between the varying water depths. (See Color Plate 4)

CLASSIFICATION

Classification is a processing technique that creates a thematic map from the bands of an image. Two pixels that both represent the same type of area could have different DN numbers due to subtle differences in the thirty by thirty meter area they represent. Classification techniques attempt to group together pixels which represent the same land cover, such as a marsh, and assign a single DN value to every pixel in that group. This DN value and all pixels that have this DN value are then associated with that type of land cover. To determine which pixels can be grouped together, they are plotted in multispectral space using each pixel's DN values as coordinates. Multispectral space is created by mutually perpendicular axes, which each represent a single TM band. There are two types of classification: unsupervised and supervised. In unsupervised classification, the algorithms determine the natural groups among the data. Supervised classification involves the analyst defining the groups and then the algorithm determines how well the data fit into them.

Unsupervised Classification Methods

This project used both isodata and single pass algorithms for the unsupervised classification. The isodata algorithm evaluates each pixels individually and assigns it to the closest initial cluster center. Once every pixel has been assigned to a cluster the computer takes each of the resulting clusters and determines its center. The algorithm then reevaluates and assigns each pixel in terms the newest centers. This process is repeated until an iteration is performed in which a specified number of pixels did not have to be reassigned to a new cluster. This percentage of pixels is the minimum convergence and is a parameter that must be set by the analyst. Other parameters specified by the analyst are the number and location of the initial cluster centers.

In contrast to the isodata, the single pass algorithm analyzes each pixel only once. The first pixel in the first row is designated as a cluster center. If the other pixels in the first row fall within a critical distance from the first pixel they are assigned to that cluster. If they exceed a critical distance they become a new cluster center. Pixels in the second and subsequent rows are grouped with a previously determined cluster center if they fall with in a specified number of standard deviations. If, however, a pixel lies beyond this number it becomes a new cluster center. In this algorithm the analyst is responsible for setting the minimum cluster size, the critical distance, and the number of standard deviations used in the algorithm.

Unsupervised Classification Results

Both types of algorithms were used in order to avoid any biasing from individual algorithm deficiencies. This project created an isodata cluster with a convergence of 98%, a minimum cluster size of 40, a distance 1 of 45, a distance 2 of 34, and a threshold of 30. (See figure 1) This resulted in a thematic map with twenty-three clusters which separated the varying water depths and sediment contents particularly well. The single pass cluster created had a minimum cluster size of 40, a critical distance 1 of 45, and a critical distance 2 of 90. (See figure 2) In contrast to the water types being clearly differentiated in the isodata, the varying land types were highlighted by the eighteen clusters resulting from the single pass.

pink to white response. The 531 image also allowed for the tracing of the sediments up stream to possible provenance. Area A and the Quaternary consolidated gravel of Burro Mesa showed very similar response. Another Quaternary gravel deposit, the Sotol Vista Overlook, spectrally matched area B. The provenance for area C may have been the pyroclastic sediments from the Tertiary Chisos Formation along the Blue Creek Canyon.

Closer observation from a ground truth of the area offered some more clues into the spectral differences in the sediments. The soil of area A ranged in size from clay particles to rock fragments 2-5 cm in length. Scrubby, brown, waist-high vegetation dominated the area. Area B soils looked similar in composition and texture, but tuff and basalt cropped out sporadically in the section. The vegetation was taller, though, and green bushes were common here. The soils of C had slightly more gravel of a finer texture than A and B, and the soil was packed much harder. Vegetation in area C was comparable to that of area A. Samples were taken from the three alluvial deposits for a lab-induced spectral response.

The plots from the x-ray diffraction show that the soils have slightly different mineral compositions. All the soils contain orthoclase and microcline, but the exact assemblage of each soil could not be determined in the time allotted. A peak search turned up numerous cards for exotic minerals, and a check using EDS spectra eliminated some on the basis of absence of necessary elements. Further treatment of the samples is needed to break down the exact components. (see fig. 1)

DISCUSSION

Through all of the processes mentioned above, the conclusion is the three drainages of the alluvial fan are different. The first major clue from the ground is the varied vegetation. Certain plants prefer to grow under specific mineralogical settings, so the differences in the plants in the areas may indicate the soils of the three drainage areas have separate provenance.

In the lab, the use of the spectra radiometer and x-ray diffraction confirmed compositional differences. The alluvial materials have slight mineralogical variance. This, probably in combination with vegetation and texture, contribute to the distinguishing spectral signatures.

The readouts of the principal components parameters gave clues to the reasons for the causes of the spectral changes from one area to another. (see fig. 2) PC band 1 gathered most information from TM bands 5 and 7, each important in detecting mineral composition. This leads one to believe that PC band 1 accentuates composition of the soils. The second PC band received the majority of its data from TM band 1 (blue light) or shadow differences. Due to this knowledge, PC band 2 is thus interpreted as a record of the texture of each soil. Finally, even though the vegetation coverage was slight, the radiation it emitted seemed to be great enough to register as PC band 3, receiving the most data from band 4, the near thermal infrared.

Component	Channel 1	2	3	4	5	7
2	0.42836	0.25816	0.42548	0.27446	0.57350	0.40571
3	0.54493	0.25166	0.38555	0.03714	-0.66040	-0.23143
4	-0.24337	0.02493	0.04566	0.85986	0.03931	-0.44403
5	-0.38334	-0.06547	0.19029	0.27637	-0.46689	0.71985
6	0.52282	-0.15951	-0.71928	0.32615	-0.11912	0.25157
7	-0.20009	0.91634	-0.33861	-0.03440	-0.03536	0.05656

Fig. 2 - Principal component eigenvectors

Using the standard Landsat image combinations (see TM 451 color plate) also yielded much information. Enhancing the images clarified the drainage systems. This clarification allows one to trace the alluvium by colors along the drainage systems back to the possible provenance. Interpretation of such is very difficult with aerial photographs or through study on the ground.

Although this study revealed some of the impact Landsat images have in geological research, much work is left to be followed up on in this project. The soils need more detailed compositional studies to isolate the exact mineralogical content. Samples from the possible provenance can also be gathered and studied with x-ray diffraction or ICP, noting if the compositions match up with the alluvium. If similarities arise, the provenance can also be studied spectrally to understand the extent of texture and vegetation altering the radiation Landsat detects. Finally, the vegetation can be studied to reveal distinct spectral signatures. The lack of time available was a main barrier from attempting these other areas of research.

REFERENCES

Sabins, F. F., 1987, Remote Sensing Principles and Interpretation, New York, W. H. Freeman and Company, 429 p.

Maxwell, R. A., 1968, The Big Bend of the Rio Grand, Austin, Texas, Bureau of Economic Geology and the University of Texas at Austin, 138 p. + Geologic map.

Supervised Classification Method

In supervised classification, the analyst groups subsets of pixels together to represent information classes such as urban, rural, etc. The algorithm then classifies all other pixels not included in the subsets, into these classes. Unsupervised classification and band combinations are used as a basis to help determine the subsets to use for the supervised classification. There are three parts of this type of classification: the training stage, the classification stage and the output image stage.

In the training stage the operator designates groups of pixels and assigns them to an information class. This is done by using the cursor to create polygons on the image that contain pixels which are representative of the desired information classes. These polygons are "training areas," for in essence they train the computer on the type of pixels should be included in the information classes created by the analyst. (See figure 3) The accuracy of the training fields is analyzed before the algorithm classifies the entire image. A graphical representation of each training field and the pixels it contains allows the analyst to see the pixels included in each field. Thus, if any fields contain pixels the analyst does not want included in the training field, the field can be redrawn before classification begins.

Once the accuracy and distribution of the training fields are satisfactory, the classification stage begins. In this stage, the computer systematically analyzes all pixels, not included in a training field, to determine which informational class they most closely resemble. Each pixel is digitally represented in a cell; these cells create an output image. The last stage of unsupervised classification produces an output image in which each pixel is color coded to represent the informational class to which it belongs.

Supervised Classification Results

In this project, the training fields were placed on a 4,3,2 image. Fifty-one training fields were created to define six informational classes: urban, marsh, rural, shallow water, mid-depth water, and deep water. The 51 training fields are dispersed through out the scene, for it is better to create many small training fields over a large area rather than a few large training fields. The overall accuracy of the training fields in this project was ninety-two percent.

URBAN GROWTH STUDY

The goal of this project was to establish the urban growth that had occurred in the area over the thirteen years between 1972 and 1985. This was determined by comparing 1972 Bureau of Economic Geology land use maps with the thematic map created from the supervised classification.

Methods

A 1972 map was scanned into the computer and imported into Canvas™. The supervised classification thematic map was also imported into Canvas™, but as a separate layer from the scanned map. The scanned map had to be rotated and scaled to fit the orientation of the classified image so that the two were coincident. The urban areas and coast of the 1972 map were traced onto a separate drawing layer in Canvas™. The thematic map and the trace layers were then imported into Adobe Illustrator™; there, trace layers were placed over the thematic map. In Canvas™ the urban area on the trace can be calculated to estimate the amount of urban area present in 1972. In order to have a contrasting figure for 1985, the number of pixels designated as urban in the thematic map was multiplied by the area occupied by each pixel (.293 by .293 km.)

Results

The result of the comparison is a thematic map overlaid with urban areas present in 1972. (See Color Plate 5) The urban area on the thematic map not covered by the overlay is clearly growth since 1972. The traced urban area from the 1972 map totaled 85.982 km^2. The 262400 pixels designated to be urban in the thematic map occupy a total area of area 225.27 km^2. Thus the increase of urban area in the Galveston area between 1972 and 1983 was 139.92 km^2. This value may be slightly higher then the actual value due to the thematic map including roads and other features in its urban classification that the urban traces of the 1972 did not. If roads and the same features were included in the 1972 calculations this value of increased urban area would likely be slightly smaller.

DISCUSSION AND CONCLUSIONS

The techniques used in the project are applicable not just to the Galveston area, but to any location being studied. These types of comparisons could also be done between two images taken at different times and extended to various land use changes, such as coastal erosion or the retreat of marshes. It is also conceivable that studies focused on bodies of water, such as their suspended sediment content or sources of sediment, could use these techniques. The advantage of using Landsat data is the multiple bands, which contain information not easily accessible, if at all, from air photos or ground mapping. The advantages of Landsat imagery make it a useful tool in land use change studies.

Color Plate 4. A 432 image of the Galveston Bay area in Texas. This composite is especially useful for highlighting vegetation and defining water and land boundaries. The bright reds and oranges indicate vegetation; the pinks and white areas, are urban and industrial sectors.

Color Plate 5. The urban trace of the 1972 map is highlighted in gray crosshatching. This trace is overlain on the supervised classification image, on which the urban area, as of 1985, is in red.

References

Barrett, E.C.; 1992; *Introduction to Environmental Remote Sensing*; Chapman & Hill; London.

Brown, L.F. Jr. (Project Coordinator); 1972; *Environmental Geologic Atlas of the Texas Coastal Zone-Galveston-Houston Area*; Bureau of Economic Geology, University of Texas at Austin; Austin, Texas.

Campbell, James B.; 1987; *Introduction to Remote Sensing*; Guilford Press; New York.

Hord, Michael R.; 1986; *Remote Sensing Methods and Application;* John Wiley and Sons Inc.; New York.

Lo, Chor Pang; 1986; *Applied Remote Sensing*; Longman; New York.

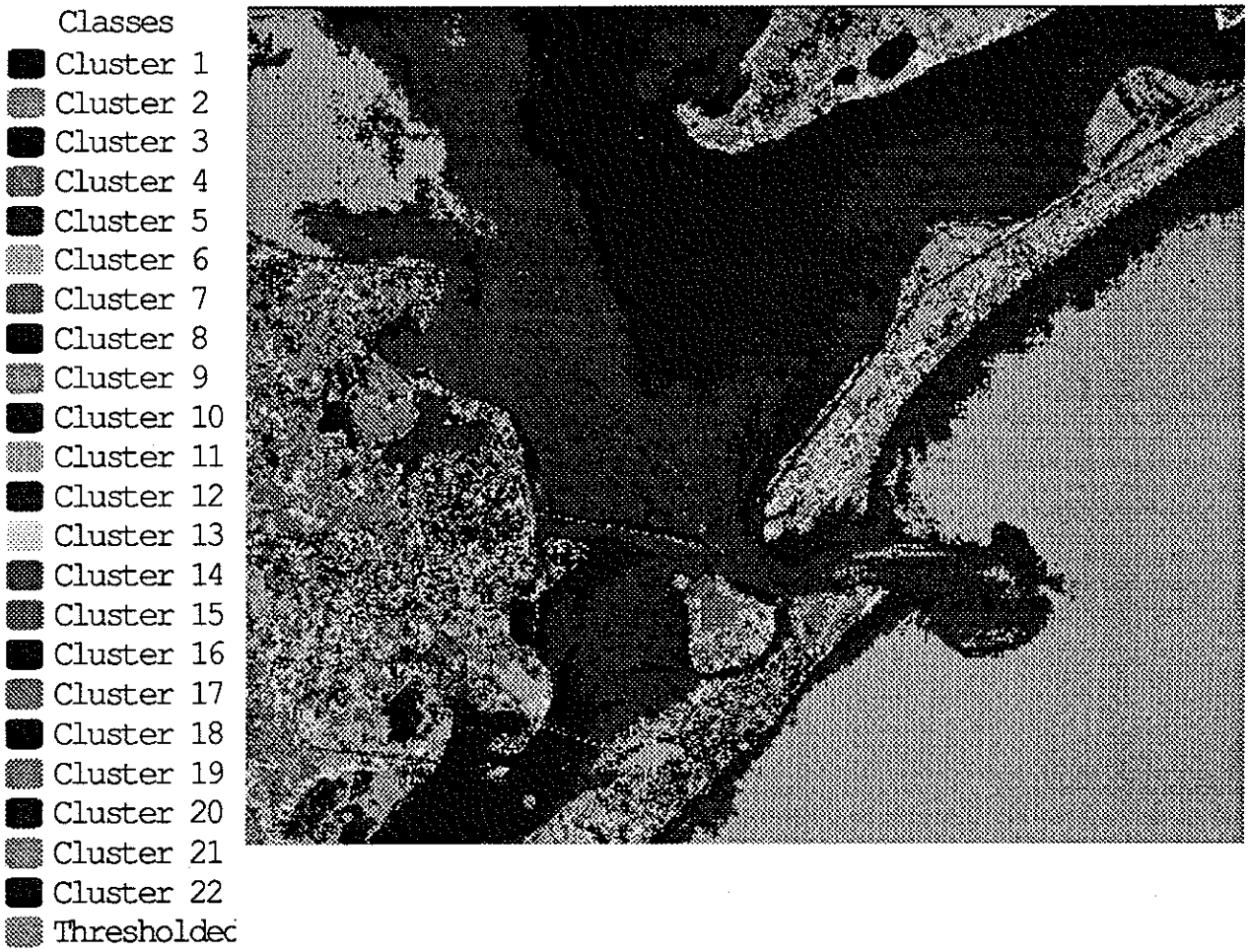

Figure 1. (Above.) Isodata cluster of the Galveston Bay area in Texas. Convergence=98%; minimum cluster size=40; distance 1=45; distance 2=34; threshold=30.

Figure 2. (Top of following page.) The single pass cluster using a minimum cluster size of 40, critical distance 1 of 45, and critical distance 2 of 90. This cluster isolates the urban area particularly well.

Figure 3. (Bottom of following page.) A selected subset of the training fields used in the supervised classification. Six information classes were used: urban, rural, marsh, shallow water, mid-depth, and deep water.

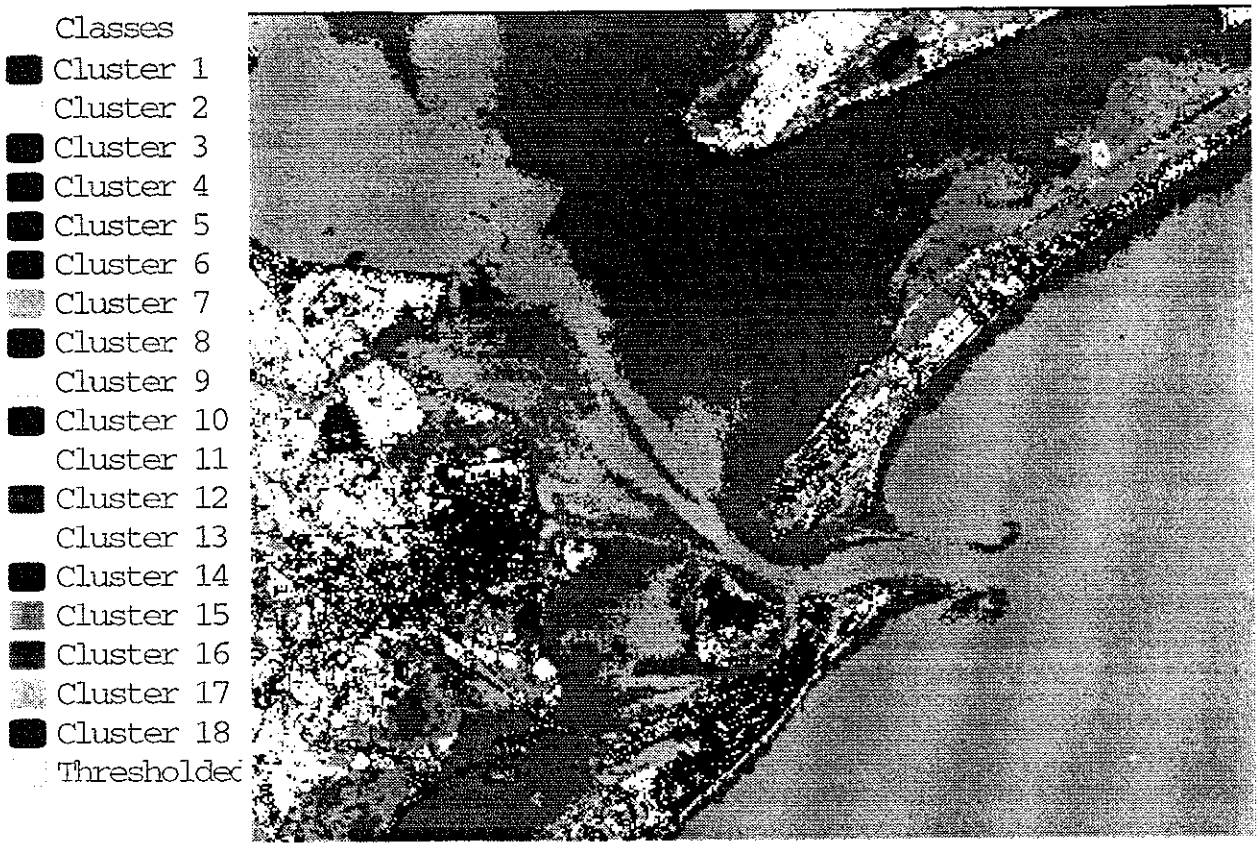
Classes
Cluster 1
Cluster 2
Cluster 3
Cluster 4
Cluster 5
Cluster 6
Cluster 7
Cluster 8
Cluster 9
Cluster 10
Cluster 11
Cluster 12
Cluster 13
Cluster 14
Cluster 15
Cluster 16
Cluster 17
Cluster 18
Thresholded

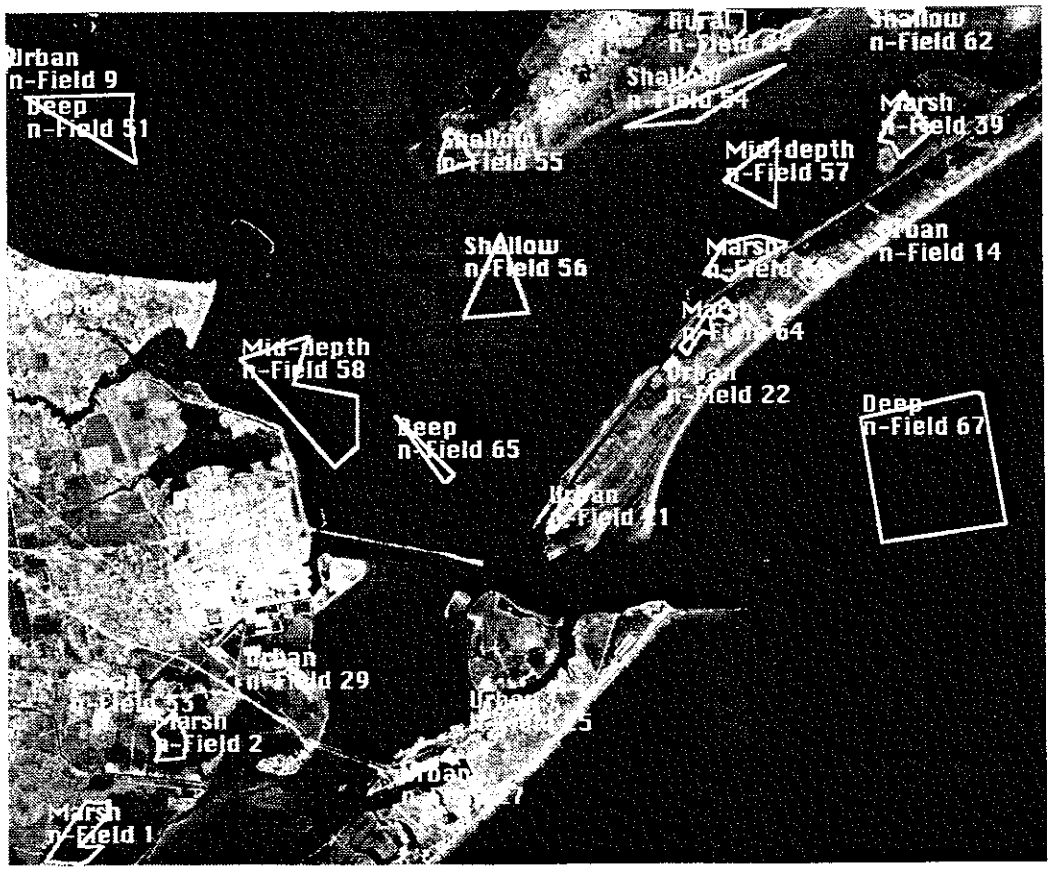
Urban
n-Field 9
Deep
n-Field 51
Shallow
n-Field 55
Shallow
n-Field 62
Marsh
n-Field 39
Mid-depth
n-Field 57
Shallow
n-Field 56
Urban
n-Field 14
Mid-depth
n-Field 58
Urban
n-Field 22
Deep
n-Field 65
Deep
n-Field 67
Urban
n-Field 29
Marsh
n-Field 2
Marsh
n-Field 1

Shoreline Changes of San Luis Pass, Texas from 1930 to 1990

Maryellen Sault
Department of Geology
SUNY College at Buffalo
Buffalo NY 14213

Rebecca Thomas
Department of Geology
Williams College
Williamstown MA 01267

Introduction

San Luis Pass is located about 45 km southwest of Galveston, Texas on the Gulf of Mexico. The pass is a tidal inlet that separates Galveston Island on the north from Follets Island on the south. It also connects the Gulf of Mexico with West Bay. Using aerial photographs (Plate 2) and a landsat image (Plate 3), we studied erosion and deposition along the north and south shorelines of San Luis Pass at approximately ten year intervals from 1930 to 1990.

Methods

Six stages were used to develop a model for shoreline evolution of San Luis Pass; (1) make a mosaic of the aerial photographs, (2) trace the shorelines as seen on the photographs, (3) reduce or enlarge the shoreline traces so that they all have the same scale and orient them so that north is at the top of the page, (4) lay the tracings for successive intervals and outline areas of erosion and deposition, (5) from these outlines computed the approximate areas of erosion and deposition and (6) graph the rates of deposition and erosion for each interval.

Aerial photographs for the years 1930, 1939, 1952, 1965, 1974, 1982, and 1990 were obtained from the Texas Bureau of Economic Geology. The photographs were used for observing the shoreline changes at San Luis Pass at approximately 10 year intervals. The entire pass was not always contained in one photograph. In order to obtain a complete picture, a mosaic was formed by using Adobe Photoshop™ 2.5. This is a process that uses two separate photographs that have common, easily identifiable features which are merged together and matched pixel by pixel. Often, the features that were to be merged together had to be rotated and cropped to line up the identified features.

To trace an outline of the shoreline, the mosaic image was transferred to Canvas™ 3.5.1. These tracings were then placed over a 1965 air photograph. (Plate 2) To fit the various shorelines to scale, easily identifiable features, such as roads, intersections and houses, were located on each photo and marked on the tracings. These were then rotated and enlarged or reduced to fit the 1965 base map. The shoreline tracings were then superimposed on the 1965 base photograph to give an overview of the changes that occurred over the whole interval. A mosaiced topographic map that was scanned into the computer to orient the shorelines north. The rulers in the program Canvas™ 3.5.1 were set to calculate the scale of these diagrams by comparing the length between common road intersections of the original map and the 1965 photograph. Two successive shoreline tracings were put together and the areas of change were outlined using Canvas™ 3.5.1. These areas were then color-coded (and patterned) to show the difference between erosion and deposition. (Figure 1.)

The areas of deposition and erosion, north and south of the pass, were then calculated for each shoreline change diagram using Canvas™ 3.5.1. To find the average deposition of each year of the interval, we summed the areas for each time span and then divided by the total number of years in the time span. Using KaleidaGraph™ 3.0.1, we graphed the average areas of deposition against time for the shorelines south and north of the pass (Figures 2a and 2b). We also added the areas of deposition north and south of the pass to produce the net total deposition of the San Luis Pass. Then, using KaleidaGraph 3.0, we graphed the net total deposition (Figure 2c). The same process was used for erosion, and plotted on the graphs with the rate of deposition.

Results

On the north shore line, the overall rate of deposition is at its highest during the interval from 1930 to 1939. It decrease during the next two blocks, with almost no deposition during the interval from 1952 to 1965. From 1965 to 1974, there is a relatively large increase in the rate of deposition, then it falls to an almost constant rate during the last two intervals. The rate of erosion is at its greatest during the interval from 1952 to 1965. The rate of erosion increased to that point and decreased to its lowest rate in the last interval. (Figures 1 and 2a)

On the south side of the inlet, there was almost no deposition during the first two intervals. There was a slight increase during the time interval from 1952 to 1965. The was a large increase in the rate of activity from 1965 to 1974. For the last two intervals, there was almost no deposition. Erosion on this side of the